CURRENT SCIENCE AND TECHNOLOGY
E-ISSN: 2785-8804
VOLUME 5, ISSUE 1, 2025, 1-10
DOI: https://doi.org/10.15282/cst.v5i1.12152

RESEARCH ARTICLE

A comparative study on the degradation of organic pollutants using green-synthesised CuO nanoparticles from clove extract and investigation of antimicrobial properties

D. Deva Angel, T. Sumitha Celin* and G. Allen Gnana Raj

Department of Chemistry and Research Centre, Scott Christian College (Autonomous), Nagercoil, Tamil Nadu 629003, India

Abstract - Nanoparticles exhibit distinct properties from their bulk materials, and they find many uses in diverse sectors of science. The use of green synthetic nanoparticles has attracted significant interest. The current study uses green-synthesized copper oxide nanoparticles from clove extract to photocatalytically degrade organic dyes, specifically Congo Red and Amido Black 10 B. Techniques such as FT-IR, UV-visible spectroscopy, EDAX, SEM, and XRD were used to characterize the produced nanoparticles. The Debye-Scherrer formula was used to determine the crystallite size. EDAX was used to confirm the presence of metal. SEM analysis was used for morphological investigations. Several factors, including catalyst dosage, dye concentration, and pH, were thoroughly examined for their effects on dye degradation. Studies on antifungal and antibacterial agents were conducted. The results revealed that the metal oxide nanocatalyst is an efficient catalyst for the degradation of organic dyes. Amido Black 10B dye degrades effectively in the presence of CuO nanoparticles synthesized from clove extract

Article History
Received : 12 March 2025
Revised : 3 May 2025
Accepted : 10 May 2025
Published : 30 June 2025

Keywords
Clove extract
Congo Red Dye
Crystallite size
Photocatalyst
Degradation
Absorption

1. Introduction

One new multidisciplinary area of study is nanoscience and nanotechnology. One of the key areas of research lately has been the green synthesis of nanoparticles, such as copper, silver, and gold, and their use. Because of their electrical conductivity, surface areas, particle size, and thermal characteristics, nanomaterials are useful in many fields [1]. The food, pharmaceutical, energy, biotechnology, and biomedicine industries all extensively use nanoparticles (NPs), a subset of nanomaterials [2]. Metallic nanoparticles are produced using a variety of physical and chemical techniques. These technologies' high levels of hazardous chemicals and needless energy use are unacceptable. To carry out NP synthesis in a reliable, cost-effective, environmentally friendly, and biocompatible manner, green chemistry and bioprocesses have been developed [3]. These nanoparticles exhibit advanced properties due to their increased surface area. In chemical technologies, eco-friendly, environmentally benign green synthesis of nanoparticles has greater advantages than the conventional method. This method of synthesis is simple, cost-effective, stable, relatively reproducible, and easily scalable for larger syntheses. Plant-based nanomaterials offer numerous benefits over traditional chemical processes and have a wide range of applications in biology and medicine. Metal oxide nanomaterials have attracted significant attention for applications across many fields due to their superior chemical, electronic, thermal, magnetic, catalytic, and optical properties compared to their bulk counterparts [4-8]. Water pollution results from the massive volume of wastewater and various effluents released by the success of contemporary businesses, particularly textile dyeing. The primary effluents that pose major risks and upset ecological equilibrium are organic dyes. This all negatively impacts animals, plants, and people. Nano metal oxides can break down these dyes.

A unique class of nanomaterials, nanostructured transition metal oxides, is used to create several innovative and intelligent materials. Because of their distinct physical and chemical properties, these transition-metal oxide nanocrystals are attracting significant attention [9–17]. The size, shape, composition, and structures of the nanocrystals all significantly impact these characteristics. The particle's surface-to-volume ratio increases as its size decreases to the nanometer range [18-19]. Due to their p-type semiconducting properties, including a narrow band gap, a monoclinic structure, and high magnetic-field resistance, research on cupric oxide (CuO) nanoparticles is currently underway [20–23]. Because of its small band gap, the CuO crystal structure exhibits practical photovoltaic and photoconductive properties [24]. Compared to micro- or bulk particles, CuO nanoparticles exhibit superior physical and chemical properties due to their large surface-to-volume ratio and smaller size. It is classified as a transition metal oxide [25]. Because of their potential uses in a variety of engineering domains, including gas sensors [26], biosensors [27], photo detectors [28], energetic materials [29], magnetic storage media [30], super capacitors [31], and photocatalysis [32], these metal oxide nanoparticles have been extensively researched.

Additionally, they serve as heterogeneous catalysts in biomedicine [33], promoting the conversion of hydrocarbons to carbon dioxide. In the present study, we synthesised CuO NPs using clove extract. They were characterised using various analytical techniques. The synthesised nanoparticles were used to degrade Congo Red and Amido Black 10B under various conditions, and the degradation efficiencies were calculated. Antimicrobial studies were also conducted on the clove extract and the synthesised CuO nanoparticles.

*CORRESPONDING AUTHOR | T. Sumitha Celin | ✉ sumithaezhil77@gmail.com

2. Methods and Material

This section covers the synthesis and characterisation of the photocatalyst. Here, the instrumentation is also covered. For the investigation, Amido Black 10B and Congo Red dyes were used. For the experiments, double-distilled deionised water was utilised. The absorption measurements were performed using the Systronics Double-Beam Spectrophotometer 2203. The emission spectra were measured using the JASCO-FP 8200 Spectrofluorometer.

2.1 Synthesis of Metal Oxide Nanoparticles

2.1.1 Preparation of clove extract

About 5 grams of the cloves were boiled with 100 mL of double-distilled water in a 250 mL beaker for about 15 minutes. It is then cooled to room temperature. The solution is filtered, and the filtrate is stored for further use.

2.1.2 Preparation of CuO NPs

A modified procedure from earlier research was used to create copper oxide nanoparticles. The clove extract was mixed with a 1:1 volume ratio of a 0.01M copper sulphate solution. Immediately after the reduction procedure, CuO NP was produced. To obtain a colloidal suspension of the nanoparticles, the liquid was magnetically agitated for 30 minutes, then left at room temperature for approximately an hour. After centrifugation and repeated water washes, the mixture was dried for approximately 2 hours at 100°C in an air oven. After calcination at 400°C in a muffle furnace, the dry nanoparticle is stored in an airtight container for further use.

2.2 Characterisation of the Photocatalyst

The produced photocatalyst was examined using FT-IR, UV-visible spectroscopy, EDAX, SEM, and XRD. To understand the structural, morphological, elemental composition, crystallite size, and functional groups, characterisation investigations were conducted. UV-visible spectroscopy techniques were used to conduct and assess the dye degradation investigations. Degradation experiments were conducted with induced light and sonication in the presence of sunshine. The pH of the dye solution was adjusted to conduct the studies.

2.2.1 Absorption spectral characteristics of nanoparticles

The absorption spectra of the solutions were used to characterise the nanoparticles produced. The amount of light extinction that occurs when light passes through a sample is measured using UV-visible spectroscopy. UV-Vis is a useful technique for identifying, characterising, and studying nanomaterials because nanoparticles exhibit special optical properties that are sensitive to size, shape, concentration, aggregation state, and the refractive index near the nanoparticle surface. The Systronics-2203 Double Beam Spectrophotometer was used to perform spectral measurements. The absorption spectra of the nanoparticles are displayed in Figure 1. Figure 1 shows the absorption maximum of the precursors, namely the clove extract, CuO nanoparticle, and the metal sulphate solution. The clove extract shows an absorption maximum of 399 nm. The precursor CuSO4 shows absorption at 398 nm, and that of CuO NP at 355 nm.

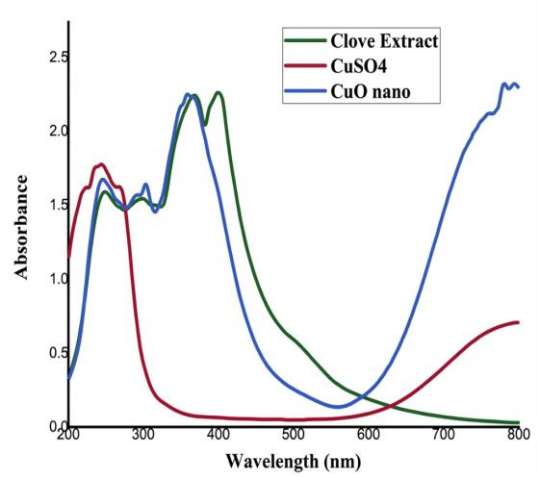

Figure 1. Absorption spectra of clove extract, CuO nanoparticle, and $CuSO_4$ solution

2.2.2 Energy dispersive X-ray analysis

Energy-dispersive X-ray analysis is also known as EDAX. Other names for it are EDS analysis and EDAX analysis. It is a method for determining a specimen's elemental composition. It is an investigation technique frequently used to characterise the elements or chemicals of items. The sample could be a liquid, a thin solid film, a solid powder, or even a pellet, among other forms. EDAX studies are used to determine the photocatalyst's elemental composition and purity.2.3) SEM and EDAX of CuO nanoparticle. Using the SEM image of the nanoparticle, its morphology was determined. These particles had a rod shape. They had a very high surface area. The SEM and EDAX are depicted in Figure 2. The EDAX spectrum confirms the presence of Cu and O, the main components of the photocatalyst. This is seen from their high weight percentage (Table 1).

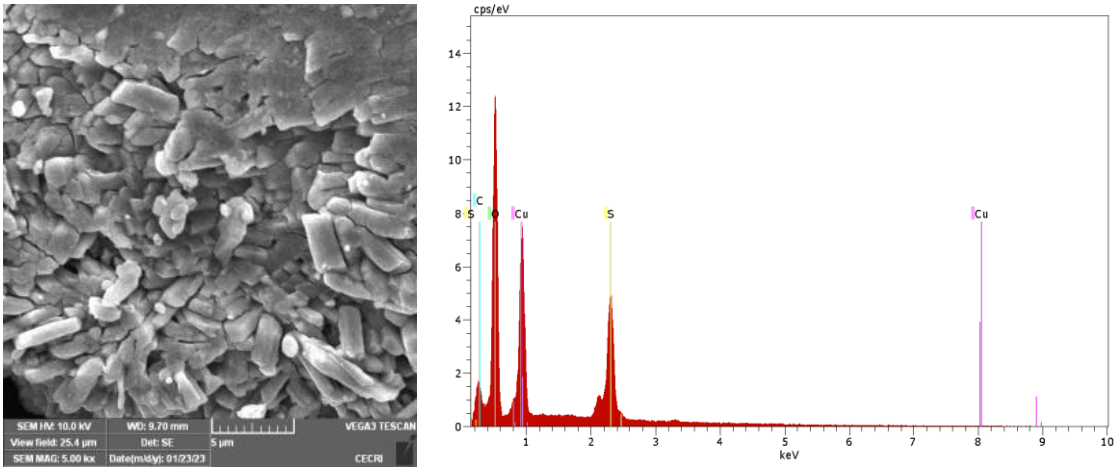

(a) (b)

Figure 2. (a) SEM image of CuO nanoparticle(b) EDAX spectrum of CuO-NPs.

Table 1. Chemical composition of CuO nanoparticle based on EDAX

Element	At. No	Series name	[wt.%]	[at.%]
O	8	K-series	40.11	55.95
Cu	29	L-series	33.59	11.80
S	16	K-series	14.30	9.95
C	6	K-series	12.00	22.30

2.2.3 XRD pattern of CuO –NPs

Figure 3 displays the XRD pattern of copper oxide nanoparticles. The peaks appeared at 2θ values ranging from 25.18°, 25.31°, 35.13°, 36. 40° and 44.58°. The peaks are in good agreement with the literature report. These diffraction peaks represent the CuO formation; the first three peaks are more intense. Furthermore, we can conclude that the produced powder is pure and free of impurities such as Cu_2O and $Cu(OH)_2$, as all the observed peaks match the monoclinic phase of CuO.

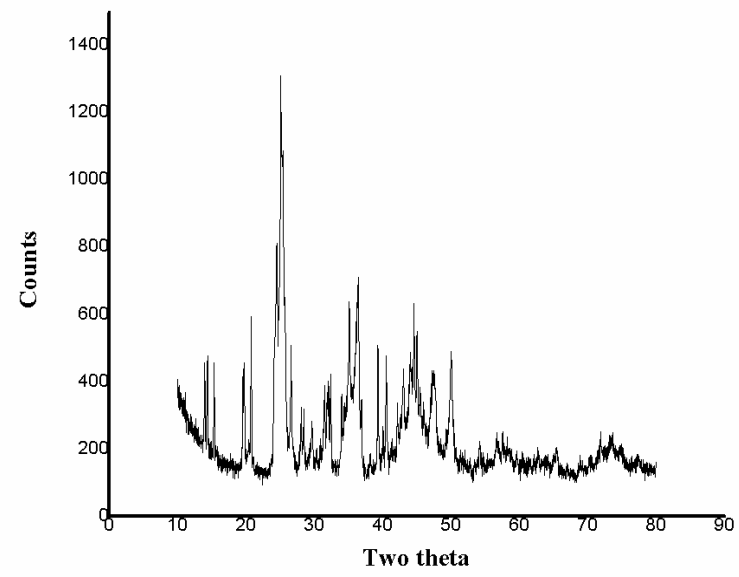

Figure 3. XRD pattern of CuO NPs

Additionally, we can match the wide contour of all peaks with the small grain size. The crystallite size was calculated using the Debye-Scherrer formula

$$D_{hkl} = \frac{k\lambda}{\beta coscos\,\theta} \quad (1)$$

where θ is the diffraction angle, β is the line's full width at half maximum (FWHM), and λ is the wavelength (λ=1.542Å) (Cu Ka). The crystallite size was found to be 19.8 nm, confirming that the synthesised product is nanoscale.

2.2.4 FT-IR analysis of the CuO nanoparticles

Figure 4 shows the FT-IR spectrum of the synthesised CuO nanoparticle. Within the 400–40,000 cm^{-1} range, FT-IR research reveals stretching vibrations at 3443.32 cm^{-1}, 2923.47 cm^{-1}, 1635.84 cm^{-1}, and 628.83 cm^{-1}. These peaks confirm the formation of CuO-NPs. The peak represents the stretching of the O-H bond at 3443.32 cm^{-1}. This peak displays both the reduction of $CuSO_4$ and the aqueous phase. The prominent peak corresponds to the Cu-O-H stretching mode at 628.83 cm^{-1}. The O-H bending vibration is represented by the peak at 1635.84 cm^{-1} [34-35].

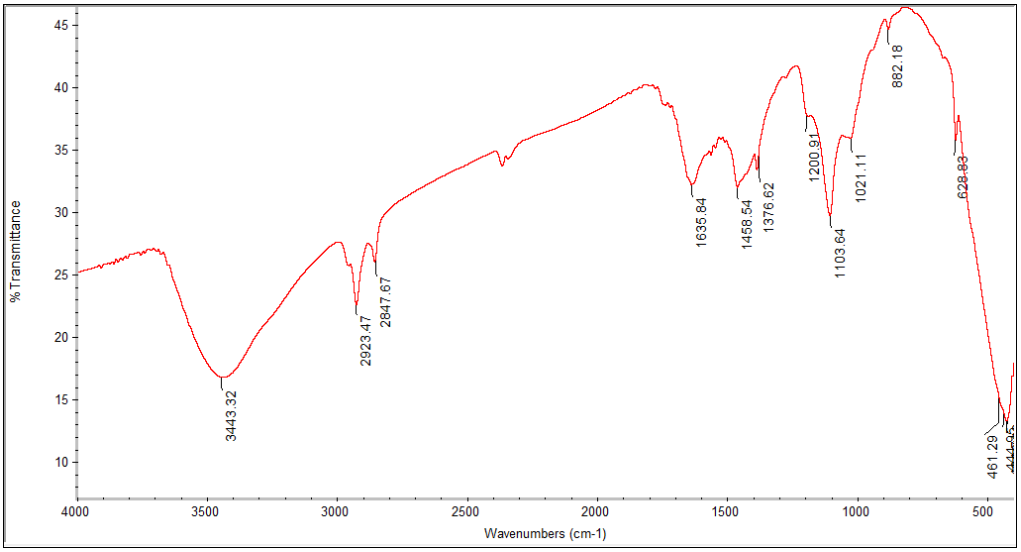

Figure 4. FT-IR Spectrum of CuO nanoparticle

3. Results and Discussion

3.1 Photodegradation Study of Congo Red Dye (CR dye) with CuO NPs

Photodegradation of the CR dye was carried out under 200 W artificial light. The reaction was carried out using 0.01g of the nanophotocatalyst and 100 mL of the CR dye. The solution was stirred using a magnetic stirrer. The absorption maximum of the dye solution was measured every half-hour. Figure 5(a) shows the absorption spectrum of Congo Red Dye. It has an absorption maximum at 532 nm. The Amido Black 10B dye has an absorption maximum of 620 nm (Figure 5(b)). The absorption maximum of the dye solution was measured every half-hour.

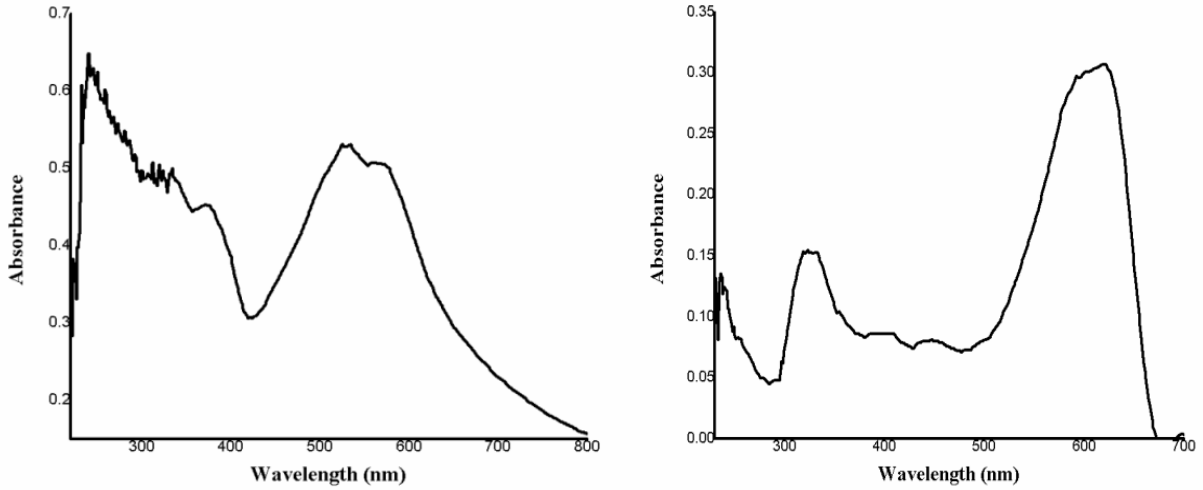

(a) (b)

Figure 5. Absorption spectrum of (a) Congo Red Dye, (b) Amido Black 10B dye

The gradual colour change from the blue of $CuSO_4$ to the brown of clove extract upon mixing the first two, producing a green colour, indicates the formation of the nanoparticle. Figure 6 shows the colour change. Figure 7 shows that the absorbance decreases with time for both dye solutions. It confirms that degradation of dye solutions occurs. The degradation of the dyes was carried out in the presence of the synthesised CuO nanoparticles, under induced light (200 W tungsten filament lamp), with a sonicator, and under sunlight. The same degradation was also carried out. Maximum degradation occurs only in the presence of sunlight and a sonicator. Figure 8 shows that absorbance decreases over time, indicating degradation.

Figure 6. Visible interpretation of colour change

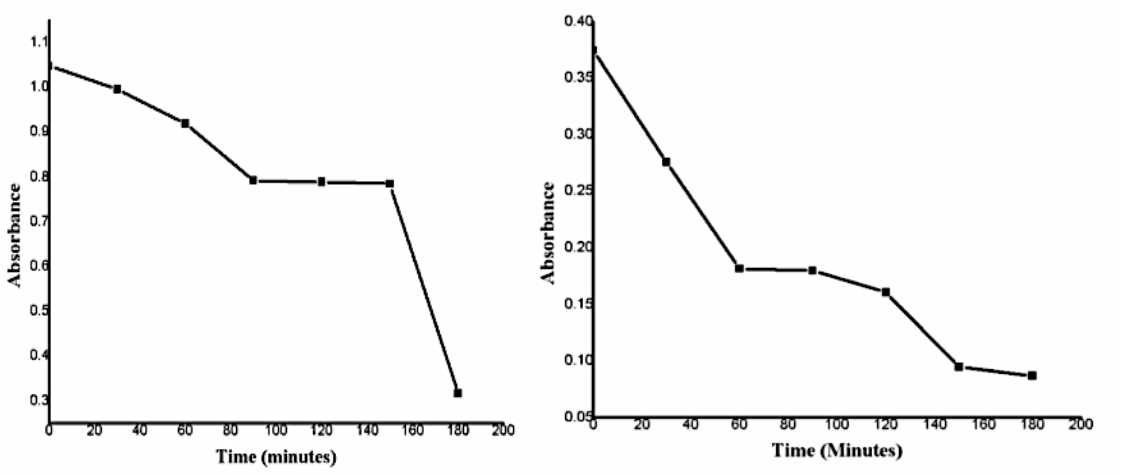

(a) (b)

Figure 7. Plot of Absorbance *vs* time for the degradation of (a) CR dye, (b) amido Black 10B dye in the presence of CuO nanoparticle

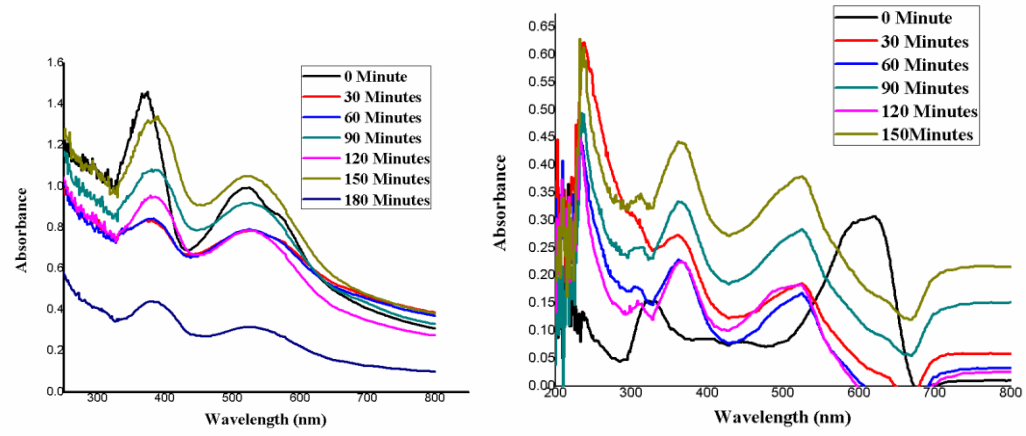

(a) (b)

Figure 8. Degradation of (a) Congo Red dye, (b) Amido Black 10B dye in the presence of CuO nanoparticles by varying the time

3.2 Effect of pH

The pH of the solution also affects the degradation of dyes. Therefore, this study was carried out by varying the pH of the dye solution. The reaction was performed at pH 2, 4, 6, 8, 10, and 12, and the degradation efficiency was calculated for each pH. The details are tabulated in Table 2 and shown in Figure 9. The pH of the solution affects the photodegradation efficiency. When the solution pH changes, the surface charge of nanoparticles is altered. As a result, the adsorption of the dye on the catalyst surface is altered, thereby altering the degradation rate. Maximum degradation at pH 2 for Congo Red dye (Table 2) and Table 3 shows Amido Black 10B degradation in the presence of CuO nanocatalyst at various pH levels. Maximum degradation occurs at pH 8. Minimum degradation occurs at pH 10. The degradation rate decreases as pH increases. This is due to the repulsion of the dye molecule and the nanoparticle. Figure 10 shows the variation in absorbance over time, along with the change in degradation percentage at different pH levels. This result indicates that the dye degrades due to changes in its pH.

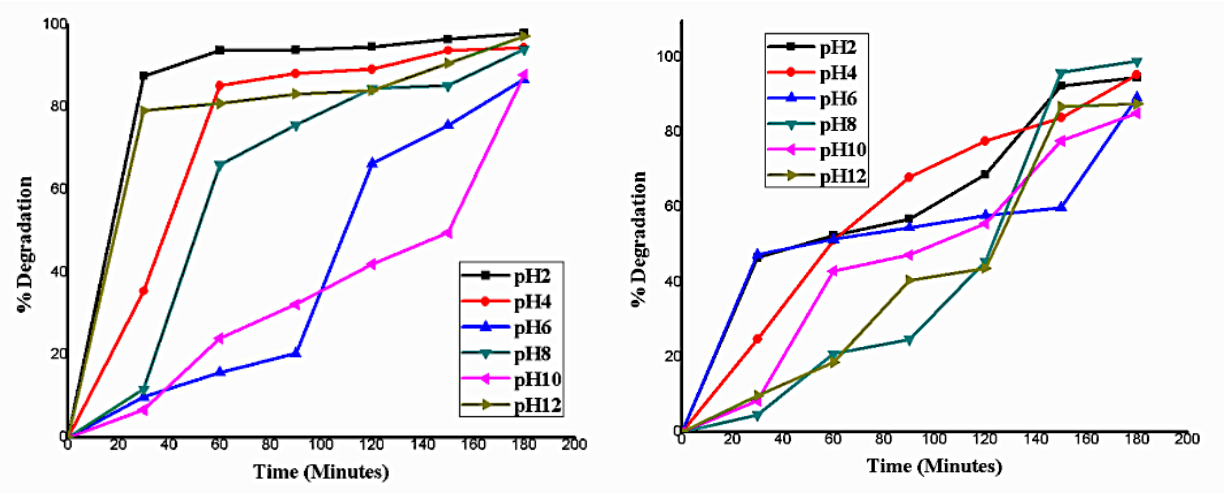

Figure 9. Degradation % of (a) Congo red dye (b) Amido Black 10B dye in the presence of CuO photocatalyst at various pH levels

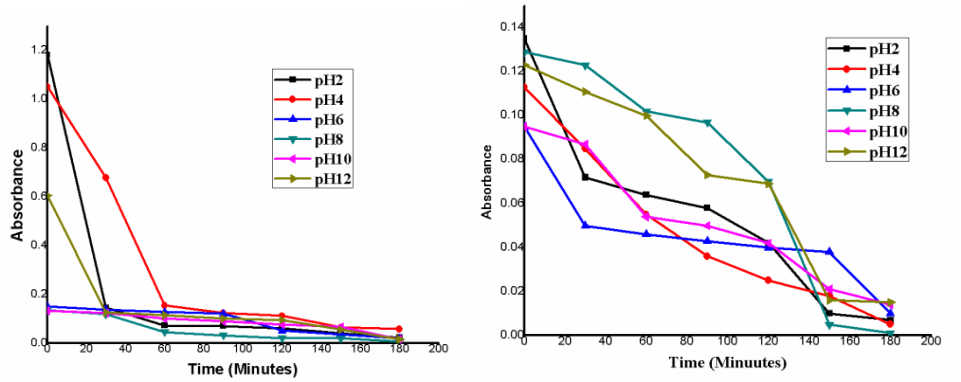

(a) (b)

Figure 10. Degradation of (a) Congo Red dye (b) Amido Black 10B dye in the presence of CuO photocatalyst at various pH levels, with change of absorbance with time

Table 2. Degradation efficiency of Congo Red dye in the presence of CuO nanoparticles at various pH levels

Time (Minute)	% Degradation					
	pH 2	pH 4	pH 6	pH 8	pH 10	pH 12
0	0	0	0	0	0	0
30	87.65850	35.51757	9.868421	11.76471	6.766917	79.20792
60	93.82925	85.28015	15.78947	66.17647	24.06015	81.0231
90	93.99831	88.22412	20.39474	75.73529	32.33083	83.33333
120	94.75909	89.26876	66.44737	84.55882	42.10526	84.15842
150	96.53423	93.82716	75.65789	85.29412	49.62406	90.75908
180	98.05579	94.49193	86.84211	94.11765	87.96992	97.35974

Table 3. Amido Black 10B degradation in the presence of CuO nanocatalyst at various pH levels

Time (Minute)	% Degradation					
	pH 2	pH 4	pH 6	pH 8	pH 10	pH 12
0	0	0	0	0	0	0
30	46.66667	24.77876	47.36842	4.651163	8.421053	9.756098
60	52.59259	51.32743	51.57895	20.93023	43.15789	18.69919
90	57.03704	68.14159	54.73684	24.8062	47.36842	40.65041
120	68.88889	77.87611	57.89474	45.73643	55.78947	43.90244
150	92.59259	84.07080	60	96.12403	77.89474	86.99187
180	94.81481	95.57522	89.47368	99.22481	85.26316	87.80488

3.3 Kinetics of the Photocatalytic Degradation of the Dye Solutions

In the presence of induced light, Amido Black 1B dye shows a maximum degradation of 76.64%, as shown in Figure 11. The photodegradation of the dyes at room temperature is shown in Figure 12. The rate constant for the photocatalytic degradation of CR dye was obtained from the first-order rate equation.

$$ln\ ln\ \frac{C_o}{C_t} = kt \quad (2)$$

where C_o and C_t are the concentrations of the dye solution at time 0 and time t in minutes. The regression coefficients for the experimental values were 0.8091 for Congo Red and 0.9785 for Amido Black 10 B. K is the first-order rate constant. This confirms that the dye molecule's degradation follows pseudo-first-order kinetics.

Amido Black 10B dye degrades at high temperatures in the presence of CuO nanoparticles. Table 4 shows the comparative results of the degradation of both dyes under various light conditions.

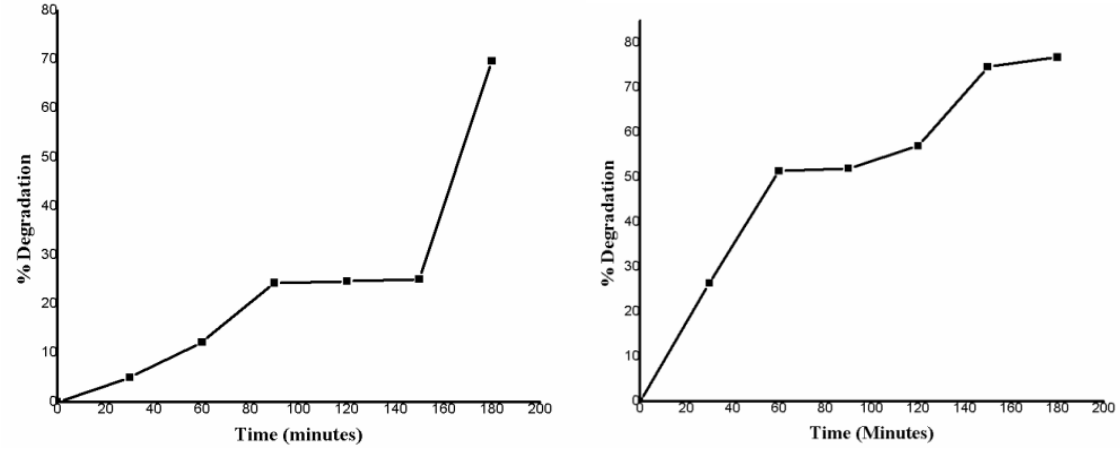

(a) (b)

Figure 11. Plot of % Degradation *vs* time for (a) CR Dye, (b) Amido Black 10B dye in the presence of CuO nanoparticle in the presence of induced light.

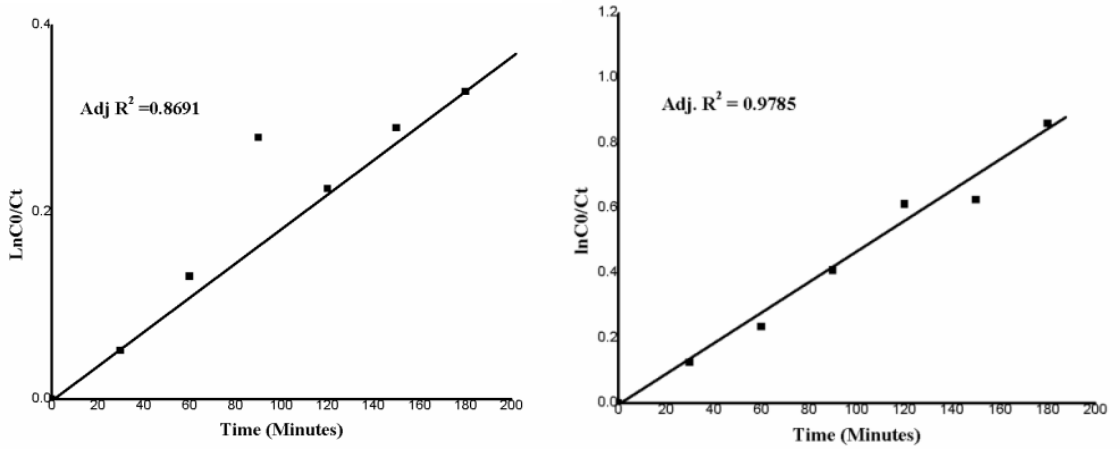

(a) (b)

Figure 12. Plot of ln Co/Ct *vs* time for (a) CR Dye, (b) Amido Black 10B dye degradation in the presence of CuO nanoparticle in the presence of induced light.

Table 4. Degradation in the presence of various light sources

	% Degradation	
Light source	Congo Red	Amido Black 10B
Induced light	69.78	76.64
Sunlight & Sonicator	98.05 (pH 2)	99.22 (pH8)

3.4 Antibacterial Activity

The well-diffusion method was used to measure antibacterial activity. A sterile petri dish was filled with 25 mL of nutritional agar. After allowing 100 µL of pathogenic bacteria to settle on the plates, they were transferred to the dish, and a sterile L rod spreader was used to form a culture lawn. A 5 mm well was made in the agar using a sterile cork borer after the pathogenic microorganisms had been incubated for 5 minutes. Wells were filled with the test samples. The

positive control was ampicillin (30 µg/mL), and the negative control was the solvent-saline-loaded well. The plates were incubated at 37 ^{O}C for 24 hours. The diameter of the zone of inhibition around the well was used to determine antibacterial activity. The antibacterial activity of the synthesised nanoparticles and the clove extract was examined using *Staphylococcus* aureus (Gram-positive bacteria) and *Escherichia coli* (Gram-negative bacteria) (Figure 13). Amicacin tablet was used as a control. The results are tabulated in Table 5. The results show that the CuO nanoparticle exhibits good antibacterial activity against both *Staphylococcus* aureus *and E. coli.* The clove extract also shows good inhibitory action against the bacterial strains.

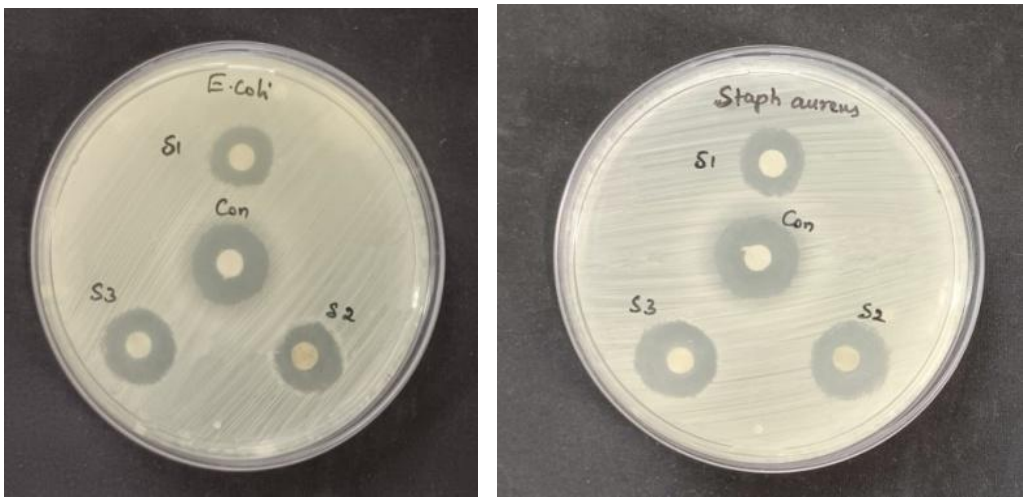

Figure 13. Antibacterial activity of the metal oxide nanoparticles against *Bacillus cereus* (Gram-positive bacteria)

Table 5. Antibacterial activity of the metal oxide nanoparticles

Bacteria name	CuO (S2)	Clove extract (S1)	Control (Amikacin)
Escherichia. coli	14 mm	16.2 mm	17 mm
Staphylococcus aureus	14 mm	17.5 mm	18 mm

3.5 Antifungal Activity

Antifungal activity was tested using the well-diffusion assay. The potato dextrose agar medium was poured into a sterile petri dish. The plates were allowed to dry. Then, 100 µL of the fungal suspension was transferred to the plate. After 5 minutes, a sterile cork borer was used to make a 5 mm well in the agar. The samples were loaded into the well, and Nystatin (30 µg/mL) served as the positive control. The plates were incubated at 37 °C for 24 to 48 hours. The antifungal activity was determined by measuring the diameter of the zone of inhibition around the well (Figure 14).

Figure 14. Antifungal activity of the metal oxide nanoparticles and clove extract

Table 6. Antifungal activity of the metal oxide nanoparticles and clove extract

S. No	Sample	Zone of inhibition
1	CuO	12.5 mm
2	Clove extract	15 mm
3	Nystatin (Control)	14 mm

Antifungal activity was assessed using the well-diffusion method. Nystatin was used as a control and is displayed in Figure 14. *Candida albicans* was the fungus used for examination. activity. The precursor clove extract shows good antifungal activity (Table 6). They have a larger zone of inhibition against the fungal stain. The bioactivities of the synthesised nanoparticles indicate that they can be used effectively in pharmaceutical applications.

4. Conclusions

Nanoparticles have many uses in many scientific domains and have unique properties compared to their bulk counterparts. The use of green synthetic nanoparticles has attracted significant interest. Clove extract was used in the current investigation for green synthesis of CuO NPs. The current study uses green-synthesised metal oxide nanoparticles to degrade organic dyes photocatalytically, specifically Congo Red and Amido Black-10 B. Techniques such as FT-IR, UV-visible spectroscopy, EDAX, SEM, and XRD were used to characterise the produced nanoparticles. Using the Debye Scherer formula, the nanoparticles' crystallite size was determined. Every measurement confirms the nanoscale size of the produced particles. The components contained in the nanoparticles were verified by XRD analysis. The manufactured nanoparticle was used in degradation experiments. Studies were conducted in a variety of settings, including a sonicator, sunshine, and induced light. Research was done on the green tea extract and the nanoparticles' antibacterial and antifungal properties. Amido Black 10B dye degrades effectively in the presence of CuO nanoparticles when exposed to light generated by the nanoparticles. It exhibits optimal efficiency. By altering the pH of the dye solution, degradation tests were conducted. At pH 8, Amido Black 10B dye degradation demonstrates a minimum efficiency of 99.23% for CuO. Because they break down a variety of textile colours, these nanoparticles are both environmentally friendly and useful for reducing pollution. The findings demonstrate that CuO nanoparticles exhibit strong antibacterial activity against E. coli and *Staphylococcus aureus.* Additionally, the clove extract exhibits strong antibacterial activity.

Acknowledgements

The authors express their gratitude to Scott Christian College (Autonomous), Nagercoil, and its Department of Chemistry & Research Centre for allowing us to complete this project.

Funding

This study was not supported by any grants from funding bodies in the public, private, or not-for-profit sectors.

Declaration of Competing Interest

The author declares no conflicts of interest.

CRediT Authorship Contribution Statement

T. Sumitha Celin and G. Allen Gnana Raj (Conceptualisation; Formal analysis; Visualisation; Supervision)
D. Deva Angel (Methodology; Data curation; Writing - original draft; Resources)

Availability of Data and Materials

The data supporting this study's findings are available on request from the corresponding author.

Ethics Declarations

This study did not involve human participants or animals. Ethical approval was therefore not required.

Generative Artificial Intelligence Declarations

The authors claim that artificially intelligent-assisted technologies, such as generative AI, were not used to generate content, ideas, or theories. We have just utilised AI to enhance readability and refine the language. This was used with extreme human control and oversight. The authors take full responsibility for reviewing and approving the content.

References

[1] J.O. Ighalo, P.A. Sagboye, G. Umenweke, O.J. Ajala, F.O. Omoarukhe, C.A. Adeyanju et al., "CuO nanoparticles (CuO NPs) for water treatment: A review of recent advances," *Environmental Nanotechnology, Monitoring and Management*, vol. 15, p. 100443, 2021.

[2] M. Ali, B. Kim, K.D. Belfield, D. Norman, M. Brennan and G.S. Ali, "Green synthesis and characterization of silver nanoparticles using Artemisia absinthium aqueous extract -A comprehensive study," *Materials Science and Engineering*: *C*, vol. 58, pp. 359–365, 2016.

[3] S.K. Das, C. Dickinson, F. Lafir, D.F. Brougham and E. Marsili, "Synthesis, characterization and catalytic activity of gold nanoparticles biosynthesized with Rhizopus oryzae protein extract," *Green Chemistry*, vol. 14, pp. 1322–1334, 2012.

[4] Q. Li, Y. Zhou and L. Zhang, "Preparation and characterization of nanoparticles through calcinations of malategel," *Materials Letters*, vol. 61, no. 8–9, pp. 1615–1618, 2007.

[5] M. Fernández-García, A. Martínez-Arias, J.C. Hanson and J.A. Rodriguez, "Nanostructured oxides in chemistry: Characterization and properties," *Chemical Reviews*, vol. 104, no. 9, pp. 4063–4104, 2004.

[6] Y.W. Jun, J.S. Choi and J. Cheon, "Shape control of semiconductor and metal oxide nanocrystals through nonhydrolytic colloidal routes," *Angewandte Chemie International Edition*, vol. 45, no. 21, pp. 3414–3439, 2006.
[7] X. Chen and S.S. Mao, "Titanium dioxide nanomaterials: Synthesis, properties, modifications, and applications," *Chemical Reviews*, vol. 107, no. 7, pp. 2891–2959, 2007.
[8] S. Laurent, D. Forge, M. Port, A. Roch, C. Robic, L. Vander Elst and R.N. Muller, "Magnetic iron oxide nanoparticles: Synthesis, stabilization, vectorization, physicochemical characterizations, and biological applications," *Chemical Reviews*, vol. 108, no. 6, pp. 2064–2110, 2008.
[9] Z.L. Wang, "Zinc oxide nanostructures: Growth, properties and applications," *Journal of Physics: Condensed Matter*, vol. 16, pp. 829–858, 2004.
[10] L. Vayssieres, "On the design of advanced metal oxide nanomaterials," *International Journal of Nanotechnology*., vol. 1, no. 1–2, pp. 1–41, 2004.
[11] E. Comini, C. Baratto, G. Faglia, M. Ferroni, A. Vomiero and G. Sberveglieri, "Quasi-one-dimensional metal oxide semiconductors: Preparation, characterization and application as chemical sensors," *Progress in Materials Science*, vol. 54, pp. 1–67, 2009.
[12] S. Dutta, S. Chattopadhyay, A. Sarkar, M. Chakrabarti, D. Sanyal and D. Jana, "Role of defects in tailoring structural, electrical and optical properties of ZnO," *Progress in Materials Science*, vol. 54, pp. 89–136, 2009.
[13] S. Barth, F. Hernandez-Ramirez, J.D. Holmes and A. Romano-Rodriguez, "Synthesis and applications of one-dimensional semiconductors," *Progress in Materials Science*, vol. 55, no. 6, pp. 563–627, 2010.
[14] J. Park, J. Joo, S.G. Kwon, Y. Jang and T. Hyeon, "Synthesis of monodisperse spherical nanocrystals," *Angewandte Chemie International Edition*, vol. 46, pp. 4630–4660, 2007.
[15] H. Zheng, J.Z. Ou, M.S. Strano, R.B. Kaner, A. Mitchell and K. Kalantar-Zadeh, "Nanostructured tungsten oxide: Properties, synthesis, and applications," *Advanced Functional Materials*, vol. 21, pp. 2175–2196, 2011.
[16] A.H. MacDonald, "Copper oxide gets charged up," *Nature*, vol. 414, pp. 409–410, 2001.
[17] Y. Liu, Y. Chu, Y. Zhuo, M. Li, L. Li and L. Dong, "Anion-controlled construction of CuO honeycombs and flowerlike assemblies on copper foils," *Crystal Growth & Design*, vol. 7, pp. 467–470, 2007.
[18] M. Vaseem, A. Umar, S.H. Kim and Y.B. Hahn, "Low-temperature synthesis of flower-shaped CuO nanostructures by solution process: Formation mechanism and structural properties," *The Journal of Physical Chemistry C*, vol. 112, pp. 5729–5735, 2008.
[19] D.I. Son, C.H. You and T.W. Kim, "Structural, optical, and electronic properties of colloidal CuO nanoparticles formed by a colloid-thermal synthesis process," *Applied Surface Science*, vol. 255, pp. 8794–8797, 2009.
[20] J.F. Xu, W. Ji, Z.X. Shen, S.H. Tang, X.R. Ye, D. Z. Jia and X.Q. Xin, "Preparation and characterization of CuO nanocrystals," *Journal of Solid State Chemistry*, vol. 147, pp. 516–519, 1999.
[21] T.H. Tran and V.T. Nguyen, "Copper oxide nanomaterials prepared by solution methods: Some properties and potential applications," *International Scholarly Research Notices*, 2014.
[22] J. Zhang, J. Liu, Q. Peng, X. Wang and Y. Li, "Nearly monodisperse Cu_2O and CuO nanospheres: Preparation and applications for sensitive gas sensors," *Chemistry of Materials*, vol. 18, pp. 867–871, 2006.
[23] A. Umar, M.M. Rahman, A. Al-Hajry and Y.B. Hahn, "Detection of nebivolol drug based on as-grown undoped silver oxide nanoparticles prepared by a wet-chemical method," *International Journal of Electrochemical Science*., vol. 8, pp. 323–335, 2009.
[24] M.M. Rahman, A.J. Ahammad, J.H. Jin, S.J. Ahn and J.J. Lee, "A comprehensive review of glucose biosensors based on nanostructured metal-oxides," *Sensors*, vol. 10, pp. 4855–4886, 2010.
[25] X. Wang, C. Hu, H. Liu, G. Du, X. He and Y. Xi, "Fast-response ozone sensor with ZnO nanorods grown by chemical vapor deposition," *Sensors and Actuators B: Chemical*, vol. 144, pp. 120–125, 2010.
[26] Y.W. Hsu, T.K. Hsu, C.L. Sun, Y.T. Nien, N.W. Pu and M.D. Ger, "Synthesis of CuO/graphene nanocomposites for nonenzymatic electrochemical glucose biosensor applications," *Electrochimica Acta*, vol. 82, pp. 152–157, 2012.
[27] F. Qu, Y. Zhang, A. Rasooly, M. Yang, "Electrochemical biosensing platform using hydrogel prepared from ferrocene modified amino acid as highly efficient immobilization matrix," *Sensors and Actuators B: Chemical*, vol. 86, pp. 973–976, 2014.
[28] S.B. Wang, C.H. Hsiao, S.J. Chang, K.T. Lam, K.H. Wen, S.C. Hung et al., "CuO nanowire infrared photodetector," *Sensors and Actuators A: Physical*, vol. 171, pp. 207–211, 2011.
[29] M.A. Dar, Y.S. Kim, W.B. Kim, J.M. Sohn and H.S. Shin, "Structural and magnetic properties of CuO nanoneedles synthesized by hydrothermal method," *Applied Surface Science*, vol. 254, pp. 7477–7481, 2008.
[30] R. Prakruthi and H.N. Deepakumari, "CuO nanoparticles: Green combustion synthesis, applications to antioxidant, photocatalytic and sensor studies," *RSC Advances*, vol. 14, pp. 28703–28715, 2024.
[31] A. Radhakrishnan and B. Beena, "Structural and optical absorption analysis of CuO nanoparticles," *Journal of the Indian Chemical Society*, vol. 2, no. 2, pp. 158–161, 2024.